Open Access

Catalysis Research

LIDSEN Publishing Inc.

Original Research

Determining the Band Alignment at the $BiVO_4$|NiOOH Interface Using the Hybrid DFT Technique

José C. Conesa *

Instituto de Catálisis y Petroleoquímica, CSIC, Marie Curie 2, 20049 Madrid, Spain; E-Mail: jcconesa@icp.csic.es

* **Correspondence:** José C. Conesa; E-Mail: jcconesa@icp.csic.es

Academic Editors: Robert S. Weber and Ali Abdelhafiz

Special Issue: Recent Advances in Electrocatalysis for Sustainable Energy and Green Chemistry

Catalysis Research
2022, volume 2, issue 1
doi:10.21926/cr.2201005

Received: November 29, 2021
Accepted: February 08, 2022
Published: February 21, 2022

Abstract

It is important to understand the band offsets between semiconductors, which are crucial to determine the direction of electron transfer at the interfaces. Two methods are normally used to determine the direction from the first principles: alternating slabs put in contact (without empty spaces between them) and separate calculations for each material surface in the presence of vacuum spaces. The first method may introduce distortions due to insufficient epitaxial match, which may lead to bandgap changes, and the second may neglect electron transfer at the interface, which may be important in systems exhibiting very different average electronegativities. This can also imply a spill of electronic density into the vacuum spaces, which will not be present at real interfaces. Herein, both approaches were used to study the $BiVO_4$/NiOOH interface, and the results were compared; the results are here relevant for photoelectrochemistry. The method is based on hybrid Density Functional Theory methods which give for the bulk phases Bandgap values that agree with the experimental ones (in one case, a value reflecting the theoretical value). The distances between the (hybrid DFT-derived) band positions and the corresponding profiles of the Hartree electrostatic potential were transferred to the interfaces. This helps determining the appropriate positions of the valence and conduction bands (as has been suggested by C. G. Van de Walle & R. M. Martin, Phys. Rev.

B 1987, 35, 8154). It is ensured that the interfaces are nonpolar (Tasker's criterion: P.W. Tasker, J. Phys. C: Solid State Phys. 1979, 12, 4977).

Keywords
$BiVO_4$/NiOOH interface; hybrid DFT methods; photoelectrochemistry

1. Introduction

$BiVO_4$ is a photocatalyst that has received considerable attention since it was first reported over 20 years ago [1]. Since its first mention, more than 3100 articles have been published on its photocatalytic properties. It is a visible light-active photocatalyst (its bandgap is $E_g \approx 2.4$ eV) and exhibits a relatively high hole mobility [2], facilitating the process of hole transport to the surface to improve the efficiency of oxidation reactions. Furthermore, it is an n-type semiconductor, which can potentially promote oxidation reactions in a photoelectrochemical setup. The electron mobility is low [3], but this can be compensated by increasing the electron concentration following the process of doping [4]. The positions of its valence and conduction bands (VB and CB, respectively) in contact with water are also known [5, 6]. This indicates that the CB lies below the NHE electrode. As it is an n-type semiconductor, its Fermi energy will be a few tenths of eV below that. This implies that H_2 production using the semiconductor will require either the application of voltage or the exploitation of a Z-scheme similar to the one observed in the case of natural photosynthesis. Analysis of the position of VB reveals that this material can be potentially used for the efficient photo-oxidation of water. A similar observation has already been reported in a paper which reported a photocatalytic reaction [1].

It has been observed that to realize an efficient photoinduced water oxidation reaction, the addition of a co-catalyst may be needed. Several co-catalysts have been reported in the literature, most of them based on Ru or Ir oxides. Hydroxides and salts of Co, Ni, or Fe have also been used as co-catalysts. One of the best co-catalysts, not based on expensive metals, is nickel oxide. Some of the (oxy)hydroxides of Ni have also been used as cheap co-catalysts [7]. This article recognizes β-NiOOH as a likely active component of the system. It has been recently reported that when Fe is used for doping, the activity of NiOOH (used for O_2 evolution) is significantly improved [8].

However, the combination of $BiVO_4$ and NiOOH has been studied only recently, and the combination has been used to realize a photoanode structure [9-12]. Methods to improve the stability of the anode in alkaline media (by saturating the solution with V^{5+} or decorating the system with TiO_2 overlayers) have been proposed [13, 14]. However, studies have not been conducted to understand to what extent the band positions of $BiVO_4$ and NiOOH favor the O_2 photo-evolution reactions at these electrodes. We used the (hybrid) DFT technique to address this issue.

2. Computational Methods

VASP (version 5.4.4) was used for data analysis [15]. The Projector augmented wave method was used [16, 17] and the valence structures $1s^1$, $2s^2 2p^4$, $3p^6 3d^5$, $3p^6 3d^{10}$, and $5d^{10} 6s^2 6p^3$ for H, O, V, Ni, and Bi, respectively, were considered. The threshold for geometry relaxation was below 10^{-4} eV in all cases. Spin polarization, i.e. full separation of spin-up and spin-down components, was used for

NiOOH. U values for V and Ni (4.0 eV and 5.3 eV, respectively) were used, and dispersion forces were taken into account [18, 19] for both materials. The known experimental value for $BiVO_4$ (E_g = 2.4 eV) was used for the calculations. For NiOOH, the value resulting in the generation of the minimum energy value (previously reported by this author; E_g = 1.45 eV) was used for the calculations [20]. The k meshes considered were (6 6 8) and (6 8 6) for $BiVO_4$ and NiOOH, respectively. Spin-orbit coupling was not considered for $BiVO_4$, as the resulting difference in the bandgap values was negligible. The HSE06 method [21, 22] was then used to adjust the experimental or theoretically computed values.

For building the interfaces, the (100) interface was considered for $BiVO_4$, as it is nonpolar according to Tasker's criterion [23]. For NiOOH, a 4x(001) interface (nonpolar according to Tasker's criterion) [23] was used. This allowed the generation of an interface of 11.70 × 5.09 Å for $BiVO_4$ and an interface of 11.30 × 5.29 Å for NiOOH. It is believed that a good epitaxial match can be obtained under these conditions as the differences are <4%. The k mesh considered for the interface (both for the combined slabs and the slabs against vacuum) was (2 1 1), and this helped simplify the calculations.

Interfaces were built following the guidelines laid down by van de Walle and Martin [24]. They determined methods to compute the Hartree potential and the experimental (or theoretically computed) values of the valence and conduction bands (in the following, VB and CB) with respect to the mentioned Hartree potential were located. Finally, a Bader analysis was carried out using the software developed by Henkelman and co-workers [25].

3. Results

3.1 $BiVO_4$

The bandgap of this material can be reproduced using HSE06, with a Fock exchange α value of 0.045. The (100) interface (which is drawn vertical and perpendicular to the plane of the drawings in all cases) is considered, and the result is shown in Figure 1a). Please note that the Hartree profile and its maximum potential are represented in black in all cases (to minimize the uncertainties attributable to inaccuracies in the grid used). The position of VB is represented in red, and the position of CB is represented in blue.

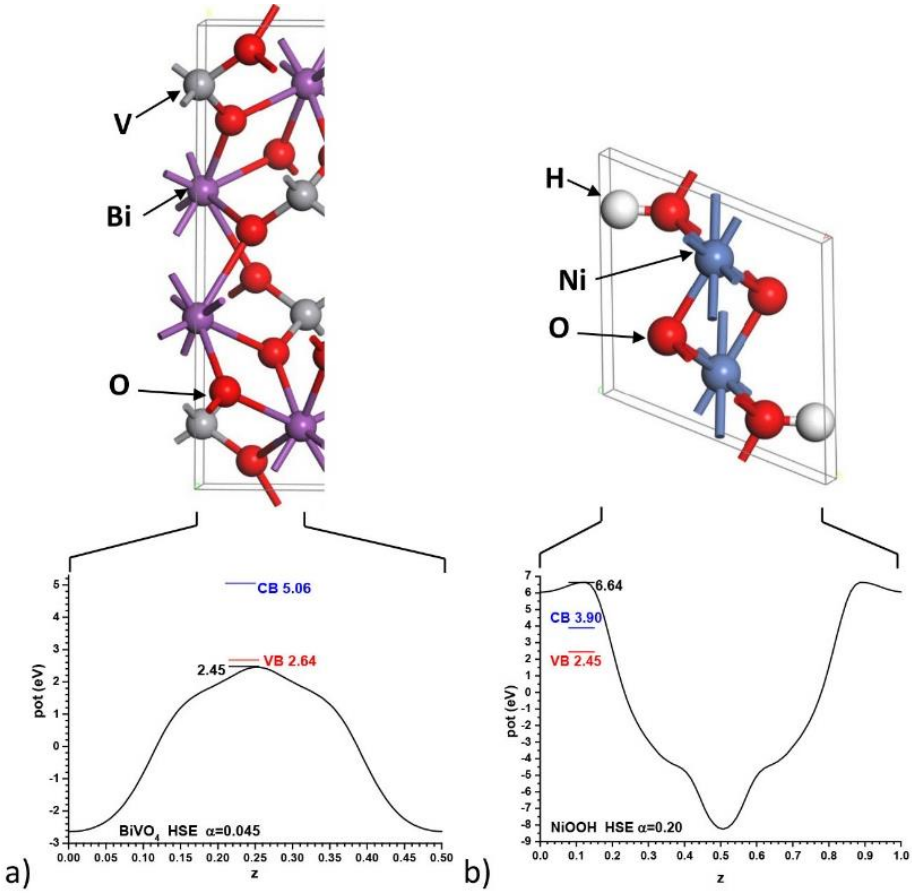

Figure 1 Positions of the Hartree potential, VB, and CB with respect to the a) $BiVO_4$ levels and b) NiOOH levels.

3.2 NiOOH

The computed bandgap, determined by analyzing the most stable case (reported previously by this author: E_g = 1.45 eV), could be reproduced using HSE06. The Fock exchange coefficient α was 0.20. The resulting Hartree potential and VB and CB positions are shown in Figure 1b).

3.3 Compound $BiVO_4$|NiOOH Interface

Eleven layers of $BiVO_4$ and five layers of NiOOH were used for the studies. Figure 2 presents the results. Only one-half of the unit cell is used as the compound slab is characterized by inversion symmetry. The figure reveals that the VB of NiOOH lies slightly above the CB of $BiVO_4$.

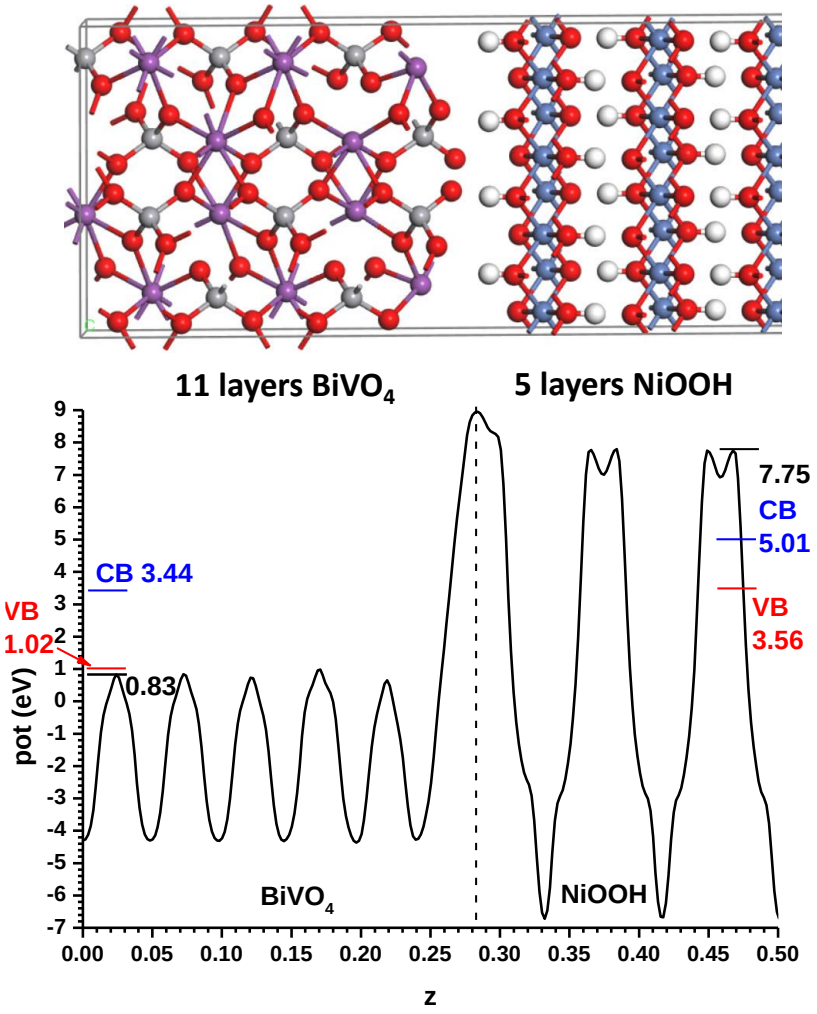

Figure 2 Results obtained for the combined slab model.

3.4 $BiVO_4$ and NiOOH Facing Vacuum

Now let us see what happens when $BiVO_4$ and NiOOH are subjected to vacuum conditions. Figure 3 presents the case where 11 layers of $BiVO_4$ and 5 layers of NiOOH are studied. Here, the dimensions in the two directions perpendicular to the interface were considered to be fixed, as they are influenced by the process of optimization of the bulk structure. The relaxation affects thus only to the direction perpendicular to the interface. Furthermore, a vacuum section of more than 10 Å was inserted in both materials, and the vacuum value was set to 0 eV. Here, the VB of NiOOH was higher than the CB of $BiVO_4$.

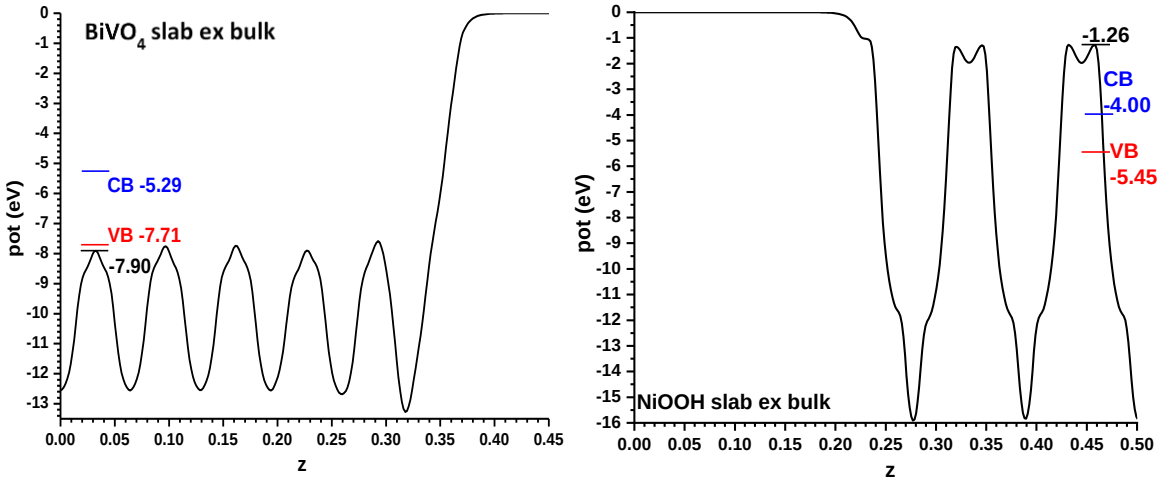

Figure 3 Positions of the Hartree potential, VB, and CB in the cases of $BiVO_4$ and NiOOH facing vacuum.

3.5 Overall Result

Figure 4 summarizes the results. It can be observed that in both cases the VB of $BiVO_4$ lies significantly lower than the VB of NiOOH. This indicates that holes generated in $BiVO_4$ (under conditions of irradiation) can be readily transferred to NiOOH, allowing the generation of O_2 in the latter. The two cases are distinctly different from each other in a crucial aspect. In the slab versus vacuum case, holes present in NiOOH can recombine with the electrons present in the CB of $BiVO_4$, while the recombination of charge carriers does not occur in the case of the combined slab. The electrons in the CB of $BiVO_4$ will then be transferred to the other electrode where they can potentially participate in the generation of H_2 or help in the generation of other reduction products.

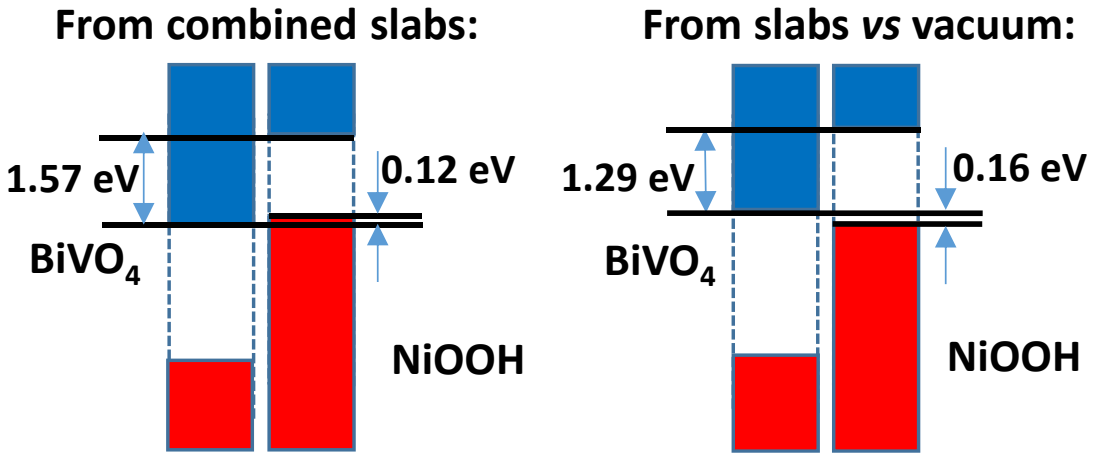

Figure 4 Comparison of the results obtained by studying the combined slabs model and the slab *vs.* vacuum model.

3.6 Analysis of Charge Densities

Next, we analyzed the charge densities. Figure 5 presents the total charge densities in the left section of the figure. The results obtained by analyzing the valence space numbers presented at the

beginning of Section 2 were considered. The differences in the densities are presented in the section to the right of the figure. The densities of each slab are subtracted from the values obtained from the combined slabs model. The atom and cell dimensions were the same as those observed in the case of the combined slabs. A transfer of charge from the NiOOH side to the $BiVO_4$ side was observed, and this agrees well with the results obtained using the combined slabs model, which predicted that transfer of charges occurred between these two sides. This result contradicts the result obtained from Bader analysis, which predicted that charge was transferred from $BiVO_4$ to NiOOH (0.011 e^- /$Å^2$). The difference in the results can be attributed to the fact that the process of Bader analysis does not take into account the asymmetry (i.e., dipoles) of charge distribution. The asymmetry is represented by the – and + signs in the right part of Figure 5. This can explain the differences in the charge distribution.

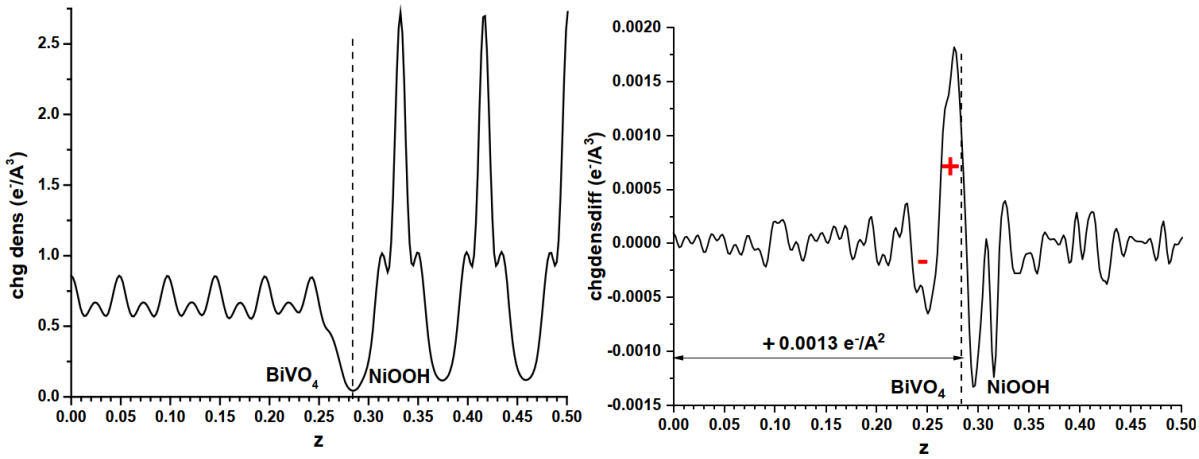

Figure 5 Total charge densities and charge density differences when each partial slab is subtracted from the overall slab.

4. Conclusions

The best model is the combined slabs model. It can be used to predict the correct direction of charge transfer (the electrons in the CB of $BiVO_4$ migrate toward another electrode). It was observed that charge transfer could not be realized when the model considered the presence of a vacuum. An inhomogeneous spill of charge can also be realized in the latter case. Such a spill can potentially be avoided when the combined slabs model is considered.

Analysis of literature reports reveals that there are other issues that need to be addressed [26, 27]. An embedding method was used in the first case, and this supported the the results obtained using the XPS X-ray Photoelectron Spectroscopy technique. Such choices are common when vacuum is taken into account. In the second case, however, a computational study was conducted using VASP and HSE06, and different results were obtained when adsorbing water (and OH^- or H^+ ions) were considered, the results being confirmed by taking experimental flat band measurements. Here, it is assumed that liquid water remains in contact with NiOOH (it may also be in contact with $BiVO_4$). Hence, it needs to be verified whether the band alignment obtained using the combined slabs model is retained. This may potentially be the subject of further work.

Acknowledgments

Thanks are given to CSIC for allowing the use of its parallel computer *trueno*, in which all the DFT calculations here were carried out.

Author Contributions

Only the present author carried out all the calculations.

Funding

This research was funded by regional project S2018/NMT-4367 (FotoArt-CM) and national project PID2019-106315RB-100 (NHyMPha).

Competing Interests

The author declares that no competing interests exist.

References

1. Kudo A, Ueda K, Kato H, Mikami I. Photocatalytic O_2 evolution under visible light irradiation on $BiVO_4$ in aqueous $AgNO_3$ solution. Catal Letters. 1998; 53: 229-230.
2. Kweon KE, Hwang GS. Structural phase-dependent hole localization and transport in bismuth vanadate. Phys Rev B. 2013; 87: 205202.
3. Kweon KE, Hwang GS, Kim J, Kim S, Kim S. Electron small polarons and their transport in bismuth vanadate: A first principles study. Phys Chem Chem Phys. 2015; 17: 256-260.
4. Bu Y, Tian J, Chen Z, Zhang Q, Li W, Tian F, et al. Optimization of the photo-electrochemical performance of Mo-doped $BiVO_4$ photoanode by controlling the metal-oxygen bond state on (020) facet. Adv Mater Interfaces. 2017; 4: 1601235.
5. Park Y, McDonald KJ, Choi KS. Progress in bismuth vanadate photoanodes for use in solar water oxidation. Chem Soc Rev. 2013; 42: 2321-2337.
6. Liu C, Luo H, Xu Y, Wang W, Liang Q, Mitsuzaki N, et al. Cobalt-phosphate-modified Mo: $BiVO_4$ mesoporous photoelectrodes for enhanced photoelectrochemical water splitting. J Mater Sci. 2019; 54: 10670-10683.
7. Briggs GW, Jones E, Wynne-Jones WF. The nickel oxide electrode. Part 1. Trans Faraday Soc. 1955; 51: 1433-1442.
8. Trotochaud L, Young SL, Ranney JK, Boettcher SW. Nickel-iron oxyhydroxide oxygen-evolution electrocatalysts: The role of intentional and incidental iron incorporation. J Am Chem Soc. 2014; 136: 6744-6753.
9. Kim TW, Choi KS. Nanoporous $BiVO_4$ photoanodes with dual-layer oxygen evolution catalysts for solar water splitting. Science. 2014; 343: 990-994.
10. Kim JH, Kaneko H, Minegishi T, Kubota J, Domen K, Lee JS. Overall photoelectrochemical water splitting using tandem cell under simulated sunlight. ChemSusChem. 2016; 9: 61-66.
11. García-Tecedor M, Cardenas-Morcoso D, Fernández-Climent R, Giménez S. The role of underlayers and overlayers in thin film $BiVO_4$ photoanodes for solar water splitting. Adv Mater Interfaces. 2019; 6: 1900299.

12. Zhu X, Liang X, Wang P, Huang B, Zhang Q, Qin X, et al. Fabrication of large size nanoporous $BiVO_4$ photoanode by a printing-like method for efficient solar water splitting application. Catal Today. 2020; 340: 145-151.
13. Lee DK, Choi KS. Enhancing long-term photostability of $BiVO_4$ photoanodes for solar water splitting by tuning electrolyte composition. Nat Energy. 2018; 3: 53-60.
14. Lee D, Kvit A, Choi KS. Enabling solar water oxidation by $BiVO_4$ photoanodes in basic media. Chem Mater. 2018; 30: 4704-4712.
15. Kresse G, Furthmüller J. Efficiency of ab-initio total energy calculations for metals and semiconductors using a plane-wave basis set. Comput Mater Sci. 1996; 6: 15-50.
16. Blöchl PE. Projector augmented-wave method. Phys Rev B. 1994; 50: 17953.
17. Kresse G, Joubert D. From ultrasoft pseudopotentials to the projector augmented-wave method. Phys Rev B. 1999; 59: 1758.
18. Klimeš J, Bowler DR, Michaelides A. Chemical accuracy for the van der Waals density functional. J Phys Condens Matter. 2009; 22: 022201.
19. Klimeš J, Bowler DR, Michaelides A. Van der Waals density functionals applied to solids. Phys Rev B. 2011; 83: 195131.
20. Conesa JC. Electronic structure of the (undoped and Fe-doped) NiOOH O_2 evolution electrocatalyst. J Phys Chem C. 2016; 120: 18999-19010.
21. Heyd J, Scuseria GE, Ernzerhof M. Hybrid functionals based on a screened Coulomb potential. J Chem Phy. 2003; 118: 8207-8215.
22. Heyd J, Scuseria GE, Ernzerhof M. Erratum: “Hybrid functionals based on a screened Coulomb potential” [J. Chem. Phys. 118, 8207 (2003)]. J Chem Phy. 2006; 124: 219906.
23. Tasker PW. The stability of ionic crystal surfaces. J Phys C Solid State Phys. 1979; 12: 4977.
24. Van de Walle CG, Martin RM. Theoretical study of band offsets at semiconductor interfaces. Phys Rev B. 1987; 35: 8154.
25. Tang W, Sanville E, Henkelman G. A grid-based Bader analysis algorithm without lattice bias. J Phys Condens Matter. 2009; 21: 084204.
26. Scanlon DO, Dunnill CW, Buckeridge J, Shevlin SA, Logsdail AJ, Woodley SM, et al. Band alignment of rutile and anatase TiO_2. Nat Mater. 2013; 12: 798-801.
27. Kullgren J, Aradi B, Frauenheim T, Kavan L, Deák P. Resolving the controversy about the band alignment between rutile and anatase: The role of OH^-/H^+ adsorption. J Phy Chem C. 2015; 119: 21952-21958.

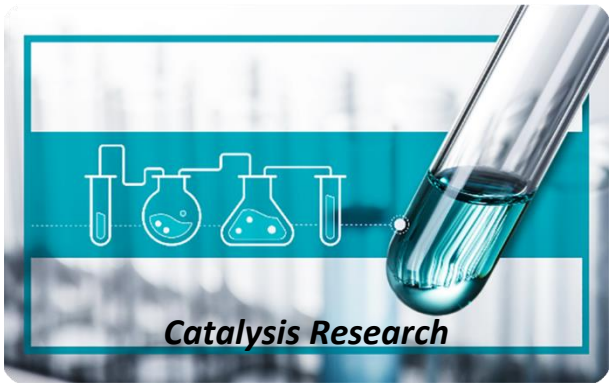

Enjoy *Catalysis Research* by:

1. Submitting a manuscript
2. Joining in volunteer reviewer bank
3. Joining Editorial Board
4. Guest editing a special issue

For more details, please visit:
http://www.lidsen.com/journals/cr